REAL TIME DYNAMIC SIMULATION OF A PAPER WINDER

by

R. Bettendorf
Metso Paper, Inc.
USA

ABSTRACT

Typically, large portions of the winder control system software are tested during the commissioning process. This is inefficient since production is shut down and financial pressures limit the time available for testing. The reason for this practice is that it is not economically feasible to integrate the winder and the electrical drive system before the installation.

Recent advances in the computational capabilities of programmable logic controllers (PLCs) have made it possible to simulate the winder, web, and drive system dynamics in greater detail than was previously possible. Shipping roll build up, parent roll build down, additional web spans, mechanical brakes, and more sophisticated drive regulation algorithms can now be simulated in real time. The increased realism allows additional control system software features to be tested before winder installation.

This paper describes a winder simulator that was used to test control system software and train operators before a new winder was installed. The simulator consisted of a dedicated PLC that solved differential equations in real time in order to model the dynamic behavior of the winder and web. The web tension and speeds of the winder model were controlled by difference equations that simulated various drive regulation algorithms. The simulator PLC used these models to provide signals for the winder PLC that would normally be supplied by the drive system and sensors on the winder.

The simulator was verified by comparing the data it generated to data from a previously installed winder. A discussion of how the simulator was used before the installation of a new winder identifies the benefits of pre-installation software testing and training.

NOMENCLATURE

b	Viscous friction of a roll
F	Tangential contact force between rolls
J	Inertia of a roll
R	Roll radius
R_{core}	Shipping roll core radius
R_{reel}	Initial parent roll radius
T	Torque
T_{brake}	Brake torque
T_{ext}	External torque (torque not due to friction)
$T_{friction}$	Torque due to friction (viscous, Coulomb, or both)
$T_{stiction}$	Stiction torque
t	Tension in a web span
V	Surface velocity of a roll
z	Average thickness of the web
θ	Angular position of a roll

Subscripts

fd	Front drum
fdb	Front drum brake
gr	Guide roll
rd	Rear drum
rdb	Rear drum brake
rr	Rider roll
sr	Spreader roll
uw	Unwind or parent roll
wu	Windup or shipping roll

INTRODUCTION

A paper winder is a multi-vendor endeavor that involves the winder manufacturer and the electric drive system supplier. Due to economic and time constraints, the winder and drive system are not integrated until the installation. Then during commissioning, the winder control software is tested with the drive system software as a complete system. This is an inefficient time to test software because production is stopped and there is a financial incentive to resume it as soon as possible. Delays caused by software errors are costly to the customer and solutions are often hastily implemented in order to speed commissioning.

Errors in control system software are caused by a variety of factors. Newly developed software inherently has a large number of errors because it has never been tested. When proven software is modified for use with a different machine, errors can be caused by changes made due to a customers unique requirements, or from unexpected interactions when two systems are integrated, or they can be typographical. Real time dynamic simulation was used to successfully find errors in the control system software of a winder rebuild before it was installed [1]. However, the model used in [1] was greatly simplified due to the limited computational capability of the programmable logic controller (PLC). The winder was modeled with a constant parent roll radius, single web span, and a windup section consisting of one speed regulated roll with no shipping roll.

The computational capabilities of modern PLCs have made it possible to increase the realism of the simulation. This paper describes a winder simulator that was able to

simulate in real time the shipping roll build up, parent roll build down, mechanical brakes, a two drum windup section, and a more sophisticated drive system model. Simulating these additional dynamic effects allowed more features of the control system software to be tested and used for operator training before the winder installation.

Three additions to the winder model are presented in the first part of this paper. They are a state variable implementation of roll radius, a mechanical brake model, and a two drum windup model. The second part of this paper gives an overview of the winder simulator and describes the winder and drive models used in the simulator program. In the third part of this paper, the results of verifying the simulator are shown by comparing the data it generated to data from a previously installed winder. This is followed by a discussion of how the simulator was used before the installation of a new winder.

ADDITIONS TO THE WINDER MODEL

Roll Radius as a State Variable

Previously, limited PLC computational capabilities resulted in the need to model a paper roll with constant radius and inertia. The desired values were selected and a simulation was run under the assumption that these parameters would vary insignificantly during the time period of the simulation. New values for the radius and inertia were selected in between simulations.

With the additional computational capabilities of modern PLCs, the radii of paper rolls can be treated as state variables and the inertias can be calculated as functions of the radii. The expression for the build up in diameter of a shipping roll as a function of velocity [2] can be easily rewritten in terms of the radius as shown in {1}.

$$R_{wu} = \sqrt{R_{core}^2 + \frac{z}{\pi}\int_0^t V_{wu}\,d\tau} \qquad \{1\}$$

However, this expression is not an efficient use of computational resources. An integration needs to be performed to find the position state and then a computationally expensive radical needs to be evaluated. The evaluation of the radical can be eliminated by using the power rule to differentiate {1} with respect to time which results in {2}.

$$\dot{R}_{wu} = \frac{zV_{wu}}{2\pi\sqrt{R_{core}^2 + \frac{z}{\pi}\int_0^t V_{wu}\,d\tau}} \qquad \{2\}$$

Substituting the radical in {2} with R_{wu} from {1} results in the state equation for the radius of a shipping roll {3}.

$$\dot{R}_{wu} = \frac{zV_{wu}}{2\pi R_{wu}} \qquad \{3\}$$

The initial value of R_{wu} is set to R_{core} and {3} can be numerically integrated to calculate the shipping roll radius. The shipping roll inertia, J_{wu}, can then be easily calculated from the radius.

The expression for the build down in radius of a parent roll as a function of velocity [3] is shown in {4}.

$$R_{uw} = \sqrt{R_{reel}^2 - \frac{z}{\pi}\int_0^t V_{uw}\,d\tau} \qquad \{4\}$$

Using the same procedure as before, the state equation for the parent roll radius can be determined {5}. R_{reel} is used as the initial value for R_{uw} and {5} can be numerically integrated to calculate the parent roll radius from which the inertia, J_{uw}, can be found.

$$\dot{R}_{uw} = -\frac{zV_{uw}}{2\pi R_{uw}} \qquad \{5\}$$

Mechanical Brake Model

In order to simulate many of the winder operating modes, such as an emergency stop or stall tension, it is necessary to have a model of a mechanical brake. Such a model would also be useful to simulate winders that control tension with a mechanical brake instead of a regenerative electric motor. However, a brake model suitable for real time simulation was not found, so a new model was developed.

The disc brakes used on winders use dry or Coulomb friction to generate braking torque. Coulomb friction models have been extensively studied in the literature [4] - [7]. Of the various models, the Karnopp model was chosen because it is simple, it lends itself well to numerical methods, and it implements a stiction region which is vital for a brake model. The Karnopp model is shown in Figure 1 with torque plotted versus velocity. There is a small stiction region near zero velocity bounded by $\pm\Delta V$. In this region, the stiction torque balances the external torque acting on the system and zero velocity is maintained. When the stiction torque is exceeded, the system enters the slip region where the retarding torque is constant regardless of velocity. The disadvantage of the Karnopp model is that it can exhibit numerical instability in the stiction region if ΔV is chosen improperly. Unfortunately, a suitable value for ΔV can be found only by trial and error.

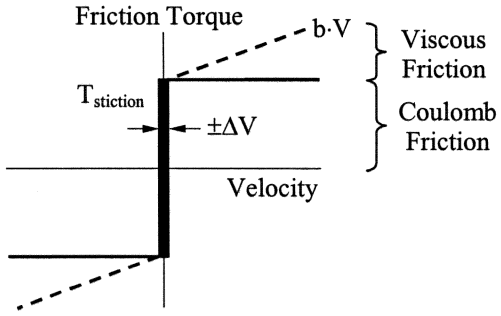

Figure 1 - Karnopp model of Coulomb friction with viscous friction.

The mechanical brake model was formed by taking the Karnopp model and adding the capability to turn the Coulomb friction on and off. The algorithm for implementing the brake model is shown in Figure 2. If the brake is turned on and the velocity is in the stiction region, the friction torque is set equal to the external torque acting on the roll

unless the brake torque is exceeded. This causes the friction torque and external torque to balance and zero velocity is maintained. In this case, the brake holds the roll back against the motor torque or web tension. If the external torque exceeds the brake torque, the friction torque is set equal to the brake torque. The difference between the external torque and brake torque accelerates the roll into the slip region. Once in the slip region, the brake torque opposes motion and viscous friction appears because the velocity is no longer zero. This time, the motor torque or web tension overcomes the brake and causes it to slip. If the brake is turned on in the slip region and the friction torque is greater than the external torque, the roll will decelerate into the stiction region where the two torques will balance. In this case, the brake causes the roll to stop. If the brake is turned off, viscous friction is the only component of the friction torque.

if *brake = on*
  // Brake is in stiction region (only Coulomb friction is present)
  if $|V| < \Delta V$
    if $|T_{ext}| < T_{brake}$
      $T_{friction} = T_{ext}$ // Friction torque equals T_{ext} and zero velocity is held
    end
    if $|T_{ext}| \geq T_{brake}$
      $T_{friction} = T_{brake} \cdot \mathbf{sign}(T_{ext})$ // Brake torque is exceeded in stiction region
    end
  end
  // Brake is in slip region (Coulomb and viscous friction are present)
  if $|V| > \Delta V$
    $T_{friction} = T_{brake} \cdot \mathbf{sign}(V) + b \cdot V$
  end
end

// Brake is off (only viscous friction is present)
if *brake = off*
  $T_{friction} = b \cdot V$
end

Figure 2 - Mechanical brake algorithm using the Karnopp model.

Another characteristic of a mechanical brake is that it does not apply and release instantaneously. The spool in the brake valve takes a finite amount of time to shift position and the pressure in the brake caliper requires time to increase or decrease. A pure time delay of 40 ms was added to the brake on/off signal to model the delay in brake application and release. This was computationally efficient because the hydraulic dynamics of the brake system did not need to be simulated.

Two Drum Windup Model

Previously, the windup was modeled as a single roll due to PLC computational limits. The models in [8] and [9] were far more complete and considered the effects of slippage and wound on tension (WOT) but they had no brakes and the rider roll was not driven. The following simplifying assumptions were used to create a suitable model:

- There is no slippage between any of the rolls in the windup
- WOT effects are negligible
- The shipping roll has uniform density
- Rolling resistance of the shipping roll acts as viscous friction
- The only effect of rider roll loading is to prevent slippage

These assumptions had varying degrees of validity, but they allowed the development of a kinetic model of the two drum windup that was computationally feasible in real time. Because of the resulting simplifications, the model can also be used with windups that have a belt bed in place of the front drum.

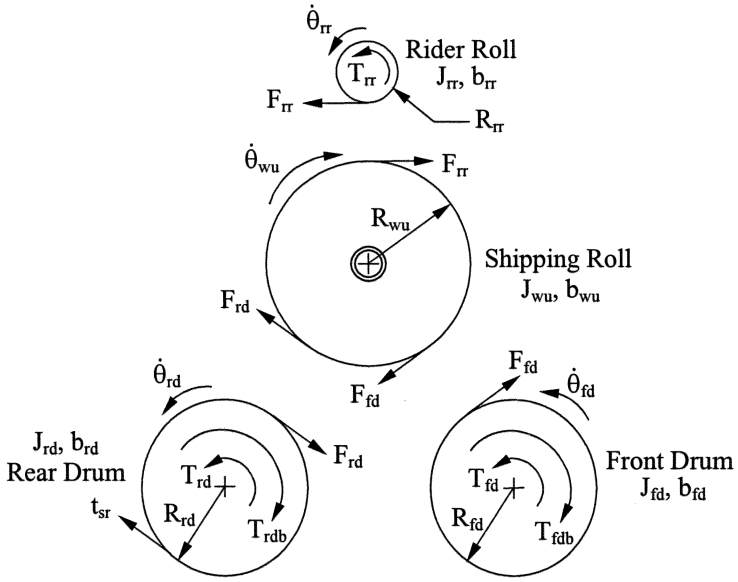

Figure 3 - Free body diagram of the windup.

The free body diagram of a two drum windup is shown in Figure 3 which includes the rear drum, front drum, shipping roll, and rider roll. Summing the moments about the center of each roll produces the equations in {6} - {9}.

$$J_{rd}\ddot{\theta}_{rd} + b_{rd}\dot{\theta}_{rd} + F_{rd}R_{rd} + t_{sr}R_{rd} = T_{rd} - T_{rdb} \qquad \{6\}$$

$$J_{fd}\ddot{\theta}_{fd} + b_{fd}\dot{\theta}_{fd} + F_{fd}R_{fd} = T_{fd} - T_{fdb} \qquad \{7\}$$

$$J_{wu}\ddot{\theta}_{wu} + b_{wu}\dot{\theta}_{wu} = (F_{rd} + F_{fd} + F_{rr})R_{wu} \qquad \{8\}$$

$$J_{rr}\ddot{\theta}_{rr} + b_{rr}\dot{\theta}_{rr} + F_{rr}R_{rr} = T_{rr} \qquad \{9\}$$

These equations can be combined to eliminate the tangential contact forces and then by rearranging results in {10}.

$$J_{rd}\ddot{\theta}_{rd} + b_{rd}\dot{\theta}_{rd} + t_{sr}R_{rd} + (J_{fd}\ddot{\theta}_{fd} + b_{fd}\dot{\theta}_{fd})\frac{R_{rd}}{R_{fd}} + (J_{wu}\ddot{\theta}_{wu} + b_{wu}\dot{\theta}_{wu})\frac{R_{rd}}{R_{wu}} + (J_{rr}\ddot{\theta}_{rr} + b_{rr}\dot{\theta}_{rr})\frac{R_{rd}}{R_{rr}} = T_{rd} - T_{rdb} + (T_{fd} - T_{fdb})\frac{R_{rd}}{R_{fd}} + T_{rr}\frac{R_{rd}}{R_{rr}} \qquad \{10\}$$

All terms in {10} can be referred to the rear drum since no slippage is assumed between any rolls. However, the angular acceleration of the shipping roll must be handled separately because its radius is a state variable. The relationship between the angular velocity of the rear drum and the angular velocity of the shipping roll is shown in {11}.

$$\dot{\theta}_{rd} R_{rd} = \dot{\theta}_{wu} R_{wu} \qquad \{11\}$$

The relationship between the angular accelerations can be found by using the product rule to take the derivative of {11} with respect to time which results in {12}.

$$\ddot{\theta}_{rd} R_{rd} = \ddot{\theta}_{wu} R_{wu} + \dot{\theta}_{wu} \dot{R}_{wu} \qquad \{12\}$$

Solving {12} for the angular acceleration of the shipping roll and referring its angular velocity to the rear drum gives the relationship in {13}.

$$\ddot{\theta}_{wu} = \ddot{\theta}_{rd} \frac{R_{rd}}{R_{wu}} - \dot{\theta}_{rd} \frac{R_{rd}}{R_{wu}} \frac{\dot{R}_{wu}}{R_{wu}} \qquad \{13\}$$

The physical interpretation of this result is that the first term on the right side of {13} represents the normal kinematic relationship between two angular accelerations. The second term on the right side of {13} is the angular deceleration of the shipping roll due to its increasing radius. Now, the remaining terms in {10} can be referred to the rear drum which results in {14}.

$$\left[J_{rd} + J_{fd}\left(\frac{R_{rd}}{R_{fd}}\right)^2 + J_{wu}\left(\frac{R_{rd}}{R_{wu}}\right)^2 + J_{rr}\left(\frac{R_{rd}}{R_{rr}}\right)^2 \right] \ddot{\theta}_{rd} +$$

$$\left[b_{rd} + b_{fd}\left(\frac{R_{rd}}{R_{fd}}\right)^2 + b_{wu}\left(\frac{R_{rd}}{R_{wu}}\right)^2 + b_{rr}\left(\frac{R_{rd}}{R_{rr}}\right)^2 - J_{wu}\left(\frac{R_{rd}}{R_{wu}}\right)^2 \frac{\dot{R}_{wu}}{R_{wu}} \right] \dot{\theta}_{rd} + t_{sr} R_{rd}$$

$$= T_{rd} - T_{rdb} + (T_{fd} - T_{fdb}) \frac{R_{rd}}{R_{fd}} + T_{rr} \frac{R_{rd}}{R_{rr}} \qquad \{14\}$$

The angular acceleration and velocity can be converted to surface acceleration and velocity by multiplying through by R_{rd}. Solving for the surface acceleration results in the state equation for the windup in {15}.

$$\dot{V}_{rd} = \left[-\left[b_{rd} + b_{fd}\left(\frac{R_{rd}}{R_{fd}}\right)^2 + b_{wu}\left(\frac{R_{rd}}{R_{wu}}\right)^2 + b_{rr}\left(\frac{R_{rd}}{R_{rr}}\right)^2 - J_{wu}\left(\frac{R_{rd}}{R_{wu}}\right)^2 \frac{\dot{R}_{wu}}{R_{wu}} \right] V_{rd} \right.$$

$$\left. - t_{sr} R_{rd}^2 + (T_{rd} - T_{rdb}) R_{rd} + (T_{fd} - T_{fdb}) \frac{R_{rd}^2}{R_{fd}} + T_{rr} \frac{R_{rd}^2}{R_{rr}} \right]$$

$$\div \left[J_{rd} + J_{fd}\left(\frac{R_{rd}}{R_{fd}}\right)^2 + J_{wu}\left(\frac{R_{rd}}{R_{wu}}\right)^2 + J_{rr}\left(\frac{R_{rd}}{R_{rr}}\right)^2 \right] \qquad \{15\}$$

THE WINDER SIMULATOR

Overview of the Simulator

The winder simulator consisted of both hardware and software. The simulation software was executed in a dedicated PLC separate from the winder PLC as shown in Figure 4. The simulator PLC provided signals for the winder PLC that are normally supplied by the drive system and various sensors located on the winder. These signals were transferred over the backplane of the chassis that the PLCs were located in. The time delay of the backplane communication simulated the serial communication delay that exists between the winder PLC and the electric drive system on an actual winder.

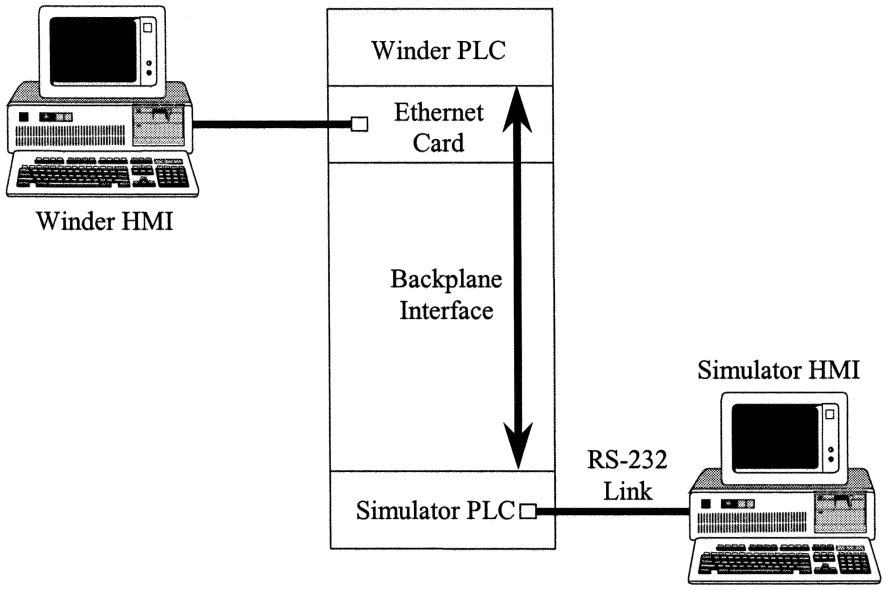

Figure 4 - Overview of the winder simulator.

The winder human-machine interface (HMI) communicated with the winder PLC through an Ethernet connection just as it would after installation. A separate simulator HMI was used to configure the models in the simulator PLC to the design specifications of a specific winder. These specifications included parameters such as inertias, frictions, diameters, and paper properties. This made it unnecessary to be familiar with the underlying mathematical models. Auto-tuning the speed regulators and the tension regulator was also initiated from the simulator HMI and performed in the simulator PLC. This eliminated the need to manually tune the regulators after configuring the models.

The Simulator Program

The program in the simulator PLC consisted of three major parts: the winder model, the drive regulator model, and the drive logic model. The winder model simulated the speeds, tensions, radii, and inertias of the winder. The drive regulator model simulated the regulators and reference generators of a generic winder drive system. The drive logic model simulated the logic of a generic winder drive system. The speeds and tension from the winder model were used as feedback to the regulators in the drive regulator model. The torques from the regulator model and the brake on/off signals from the drive logic model were inputs into the winder model.

The winder model consisted of a system of non-linear differential equations that simulated the dynamics of the rolls and web spans. The models developed earlier in this paper were used along with the primitive elements described in [10] to create the model shown in Figure 5. Web breaks were modeled by forcing all tension states to zero when the ultimate tensile strength of any web span was exceeded or when the parent roll ran out of paper. Even though a modern PLC was being used, some simplifications were made. Three guide rolls and two slitter table rolls that had the same radii were assumed to have the same angular acceleration. This allowed them to be lumped together into one roll with an inertia equal to the sum of their individual inertias. Two spreader rolls were lumped together in the same manner. Reducing the number of rolls and web spans reduced the order of the model and its computational requirements. The differential equations of the winder model were solved in real time with a fourth order Runge-Kutta algorithm. A task in the PLC containing the model was executed every 4 ms and the step size of the Runge-Kutta algorithm was set equal to 4 ms. The task execution rate and step size were made equal to scale the simulation time to correspond to actual time.

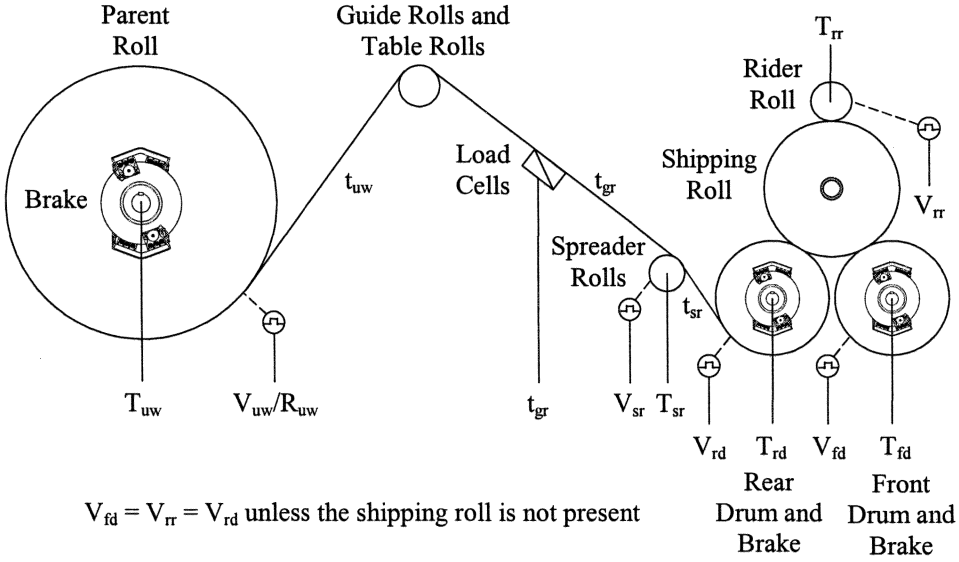

Figure 5 - Winder model.

Figure 6 shows a simplified diagram of the drive regulator model. The control strategies in [11] were used along with a proprietary winding force control strategy for the front and rear drums. These strategies used inertia compensated proportional-integral speed and tension regulators implemented with difference equations. The references were generated by the model using setpoints from the winder control software. The torque regulators were assumed to be ideal because in modern drives they have a very high bandwidth. This implied that the motor shaft torques were instantaneously equal to the torque references. In addition, the regulator model was not allowed to access the winder model parent roll radius or surface velocity states. The parent roll diameter was estimated with the same method as an actual drive system. An initial diameter preset was used along with the ratio between the rear drum surface velocity, V_{rd}, and the unwind motor rotational velocity, V_{uw}/R_{uw}. The parent roll surface velocity and inertia were estimated in the regulator model using this diameter. A task in the PLC containing the model was executed every 10 ms and the step size of the difference equations was set to 10 ms. As before, this was done to scale the simulation time to correspond to actual time.

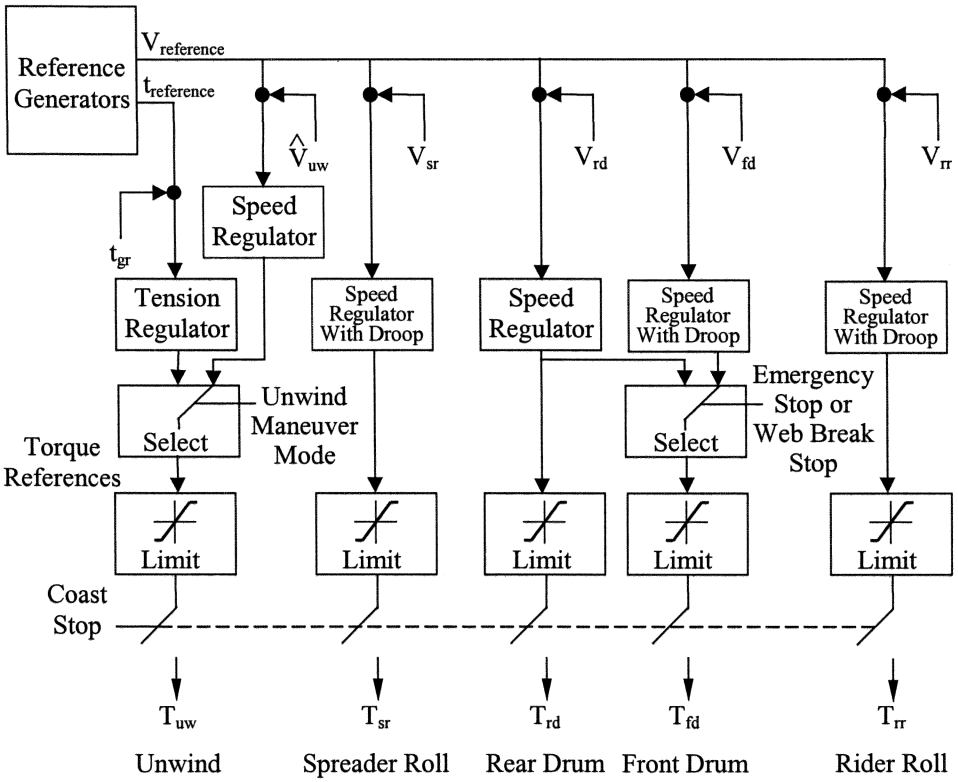

Figure 6 - Drive regulator model.

The drive logic model was used to provide interlocking to select the different operating modes such as unwind maneuver, thread, run, normal stop, emergency stop, coast stop, and web break stop. Each mode caused different speed and tension references to be followed, turned brakes on or off, and caused the drive regulator model to switch between different control strategies. The logic model also simulated the communications interface between the drive system and the winder PLC by transferring signals over the chassis backplane. The logic model was implemented in a task that ran continuously and was interrupted by the two real time simulation tasks mentioned earlier.

RESULTS

Simulator Verification

Figures 7 - 14 compare the data from the winder simulator to data from an existing winder. The actual and simulated winder speeds are virtually identical as shown in Figures 7 and 8. The only difference is that the actual speed starts at thread speed while in the simulation, the winder starts at zero speed and accelerates to thread speed.

Figures 9 and 10 compare the web tension of the span between the guide rolls and spreader rolls. In both data sets, tension disturbances can be seen whenever the winder changes speed. There are some additional disturbances present in the actual winder tension that are not present in the simulation. This can be attributed to the fact that some web spans were combined and some rolls were lumped together into equivalent rolls in the winder model. This simplification eliminated some of the web tension dynamics in the simulation. Also, because roll eccentricity was not modeled, the simulated tension

did not have a low amplitude, high frequency noise component like the actual tension. The steady state error in the actual tension was caused by an improper compensation in the unwind drive for the wrap angle of the web on the tension roll (a slitter table roll mounted on load cells).

Figures 11 and 12 compare the drum torques of the windup section. The dynamics of the actual and simulated torques are very similar. However, there is a difference in magnitude that is not speed related. This indicates that it is not caused by large errors in the values of viscous friction. The difference is most likely caused by the many simplifying assumptions used in the windup model along with the improper compensation in the unwind drive of the actual winder.

The shipping roll and parent roll diameters estimated by the actual drive system and winder control system are shown in Figure 13. Figure 14 shows the parent roll diameter estimated by the drive regulator model. The shipping roll diameter in Figure 14 is the state variable, R_{wu}, calculated in the winder model multiplied by two. Although the actual and simulated diameters appear to be identical, there is a small difference between them. This is because the windup model assumes uniform density in the shipping roll and ignores WOT effects. The model of the parent roll also assumes uniform density which affects the accuracy of its diameter. At the start of the data, a small spike can be seen in the simulated parent roll diameter. The diameter estimator in the drive regulator model needs additional interlocking to prevent this since the state variable, R_{uw}, in the winder model does not produce this spike.

While there are some differences between the actual winder data and the simulated winder data, it can be seen that most of the dynamic phenomena were properly captured by the simulation. This allowed the winder simulator to be used as an effective tool for saving time and costs by verifying winder control software and training operators.

Results of Using the Simulator

One benefit of the winder simulator appeared early in the project when an error was unexpectedly found during its development. A proprietary drive specification was used as a reference to write the drive logic in the simulator program. The specification contained an incorrect description of tension detection.

After the simulator was developed, it was connected to the PLC and HMI for a new winder as shown previously in Figure 4. The winder model was configured to the design specifications of the winder and the regulators in the drive model were auto-tuned. The winder PLC and HMI software were then tested and 22 errors were discovered. It required 24 hours of testing to find and correct these errors. Testing during the commissioning process takes longer because the entire winder is not always available for troubleshooting, the drive vendor and the winder vendor are not always available to work on an error simultaneously, and both vendors are typically separated by some distance due to equipment location. Therefore, it was estimated that using the winder simulator for control software testing saved 36 hours of actual commissioning time.

The simulator was also used during operator training after the winder control software was tested. Normally, the operators would train using just the winder HMI to change from one static screen to another. With the simulator, the winder HMI displayed realistic operating conditions that the operators could manipulate. For example, if the parent roll diameter preset for the unwind drive was not set equal to twice the radius in the winder model, the drive regulator model would calculate the incorrect torque and inertia compensation. This could lead to a web break on start up just as it would on a real winder. In addition, the operators were able to use some of the advanced winder control software features such as data trending and automatically stopping the winder based on roll diameter or length. These capabilities gave the operators a better opportunity to learn how the actual winder would perform.

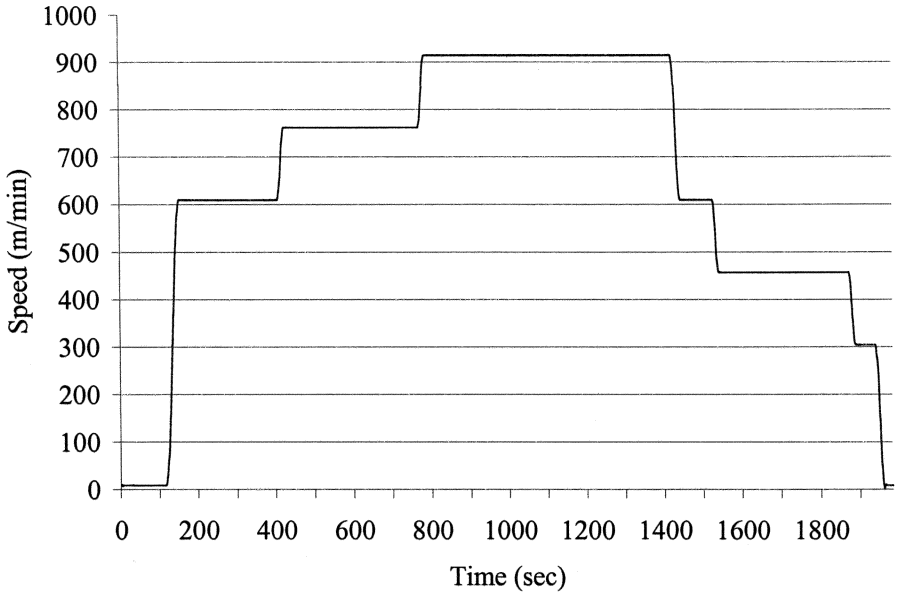

Figure 7 - Actual winder speed.

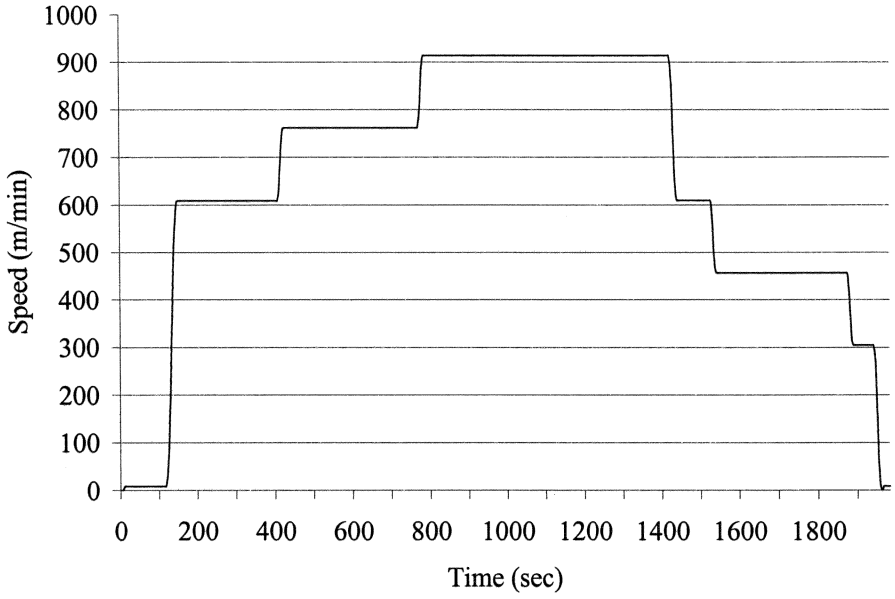

Figure 8 - Simulated winder speed.

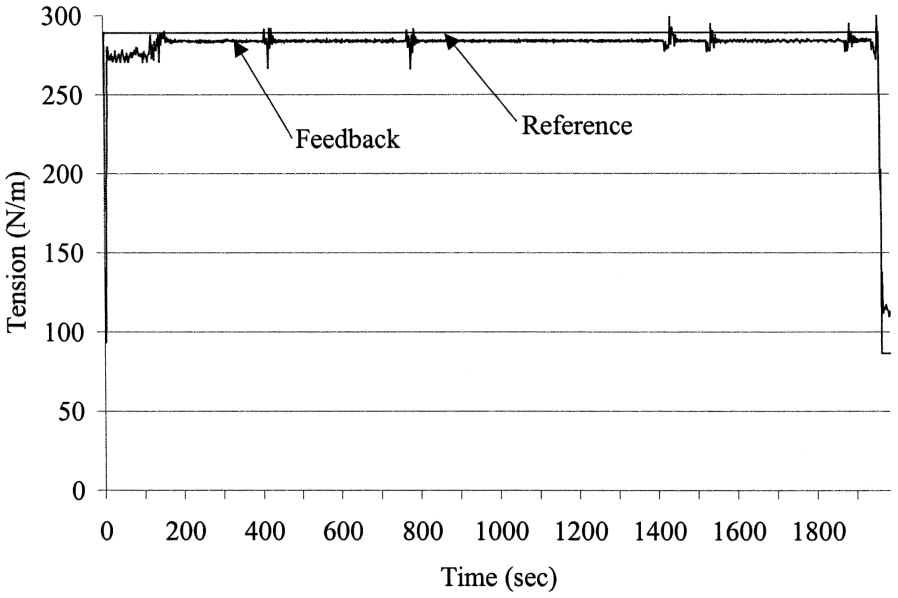

Figure 9 - Actual web tension feedback and tension reference.

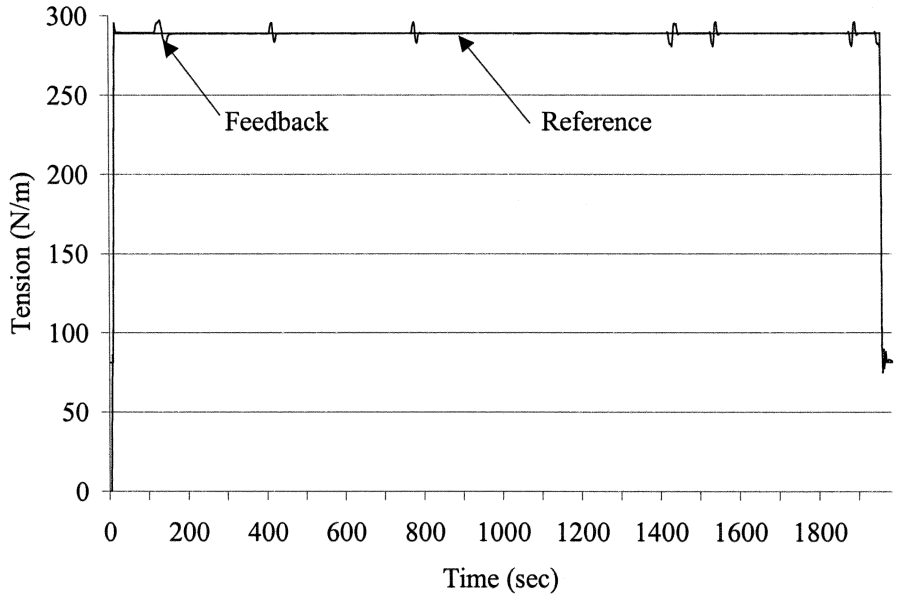

Figure 10 - Simulated web tension feedback and tension reference.

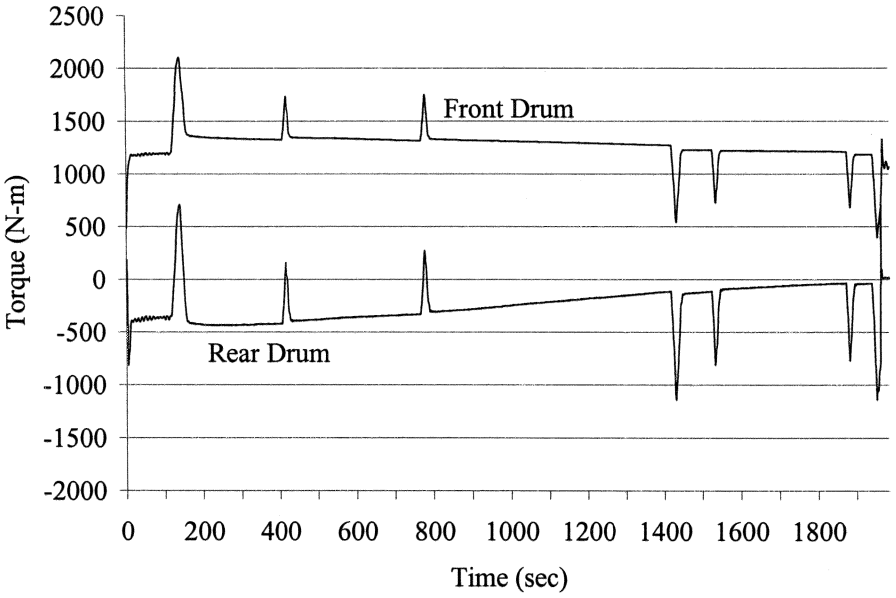

Figure 11 - Actual winder drum torques.

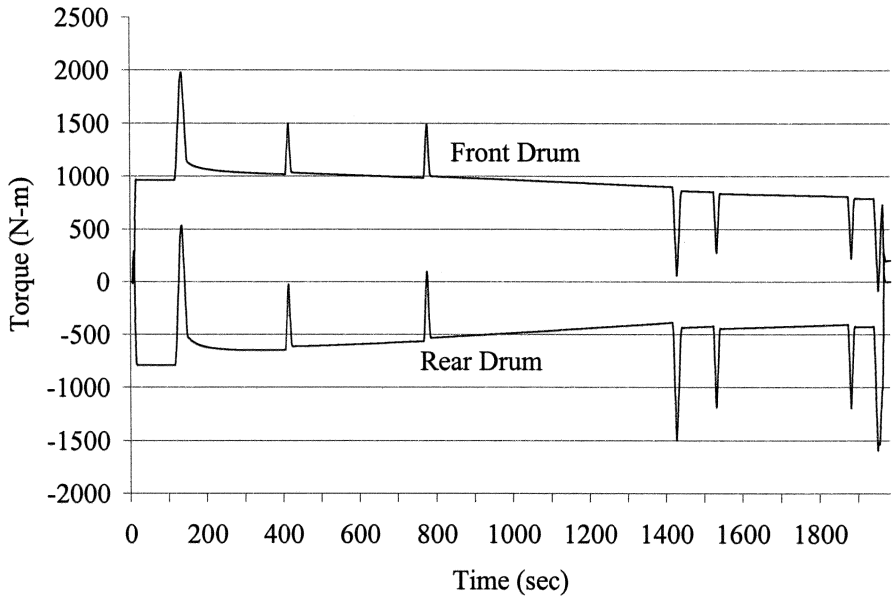

Figure 12 - Simulated winder drum torques.

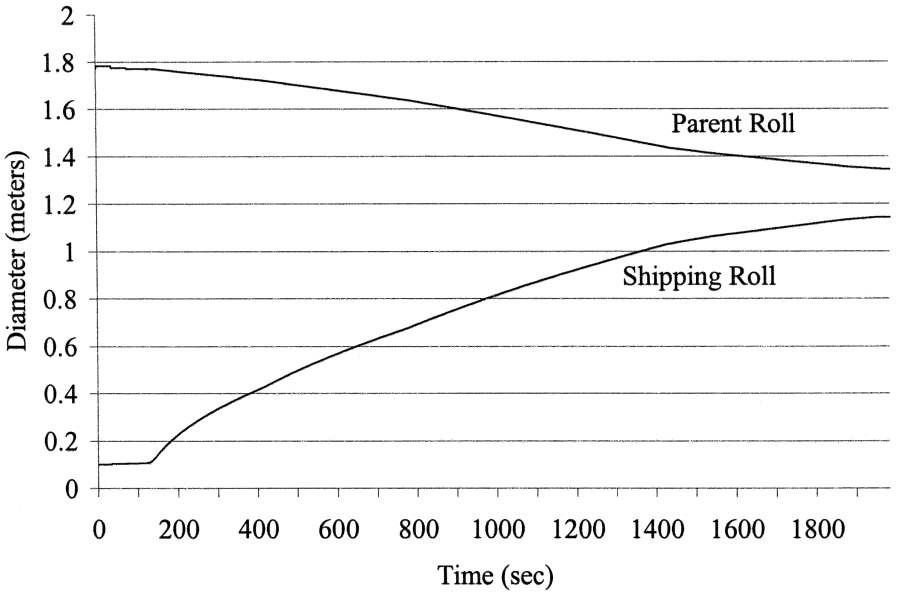

Figure 13 - Actual winder paper roll diameters.

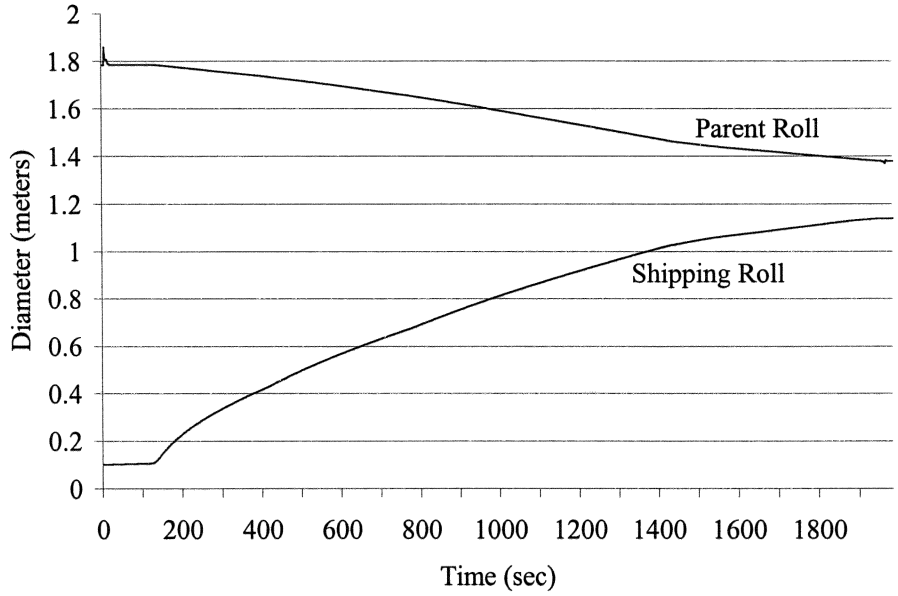

Figure 14 - Simulated winder paper roll diameters.

CONCLUSION

This paper described a winder simulator that took advantage of advances in the computational power of modern PLCs to produce a more realistic simulation. The simulator was verified with data from an existing winder and was used both to successfully test the software of a new winder and to train its operators.

As the computational power of PLCs continues to increase, additional phenomena could be simulated. This includes more realistic rider roll loading effects, slippage in the windup, and the effects of WOT on the shipping roll. Another improvement would be to find a Coulomb friction model for use in the mechanical brake model that does not exhibit numerical effects depending on the choice of ΔV.

ACKNOWLEDGMENTS

The author would like to thank Mel Kruse for his constant encouragement and Kurt Dietzen for providing the opportunity to demonstrate the capabilities of this work.

REFERENCES

1. Bettendorf, R., "Real Time Dynamic Simulation For Control System Software Verification", Proceedings of the Sixth International Conference on Web Handling, Oklahoma State University, Stillwater, Oklahoma, June 10-13, 2001.

2. Jorkama, M. and Von Hertzen, R., "Two-Drum Winder Run Simulation Model", Proceedings of the Fourth International Conference on Web Handling, Oklahoma State University, Stillwater, Oklahoma, June 1-4, 1997.

3. Song, S. and Sul, S., "Design and Control of Multispan Tension Simulator", IEEE Transactions on Industrial Applications, Vol. 36, No. 2, pp. 640-647, Mar./Apr. 2000.

4. Johnson, C. T. and Lorenz, R. D., "Experimental Identification of Friction and Its Compensation in Precise, Position Controlled Mechanisms", IEEE Transactions on Industrial Applications, Vol. 28, No. 6, pp. 1392-1398, Nov./Dec. 1992.

5. Chen, B. C., Tilbury, D. M., and Ulsoy, A. G., "Modular Control For Machine Tools: Cross-Coupling Control With Friction Compensation", Proceedings of the ASME, Dynamic Systems and Control Division, DSC Vol. 64, pp. 455-462, 1998.

6. Dupont, P., Armstrong, B., and Hayward, V., "Elasto-Plastic Friction Model: Contact Compliance and Stiction", Proceedings 2000 American Control Conference, pp. 1072-1077, Chicago, Illinois, June 28-30, 2000.

7. Leine, R. I., Van Campen, D. H., and De Kraker, A., "Stick-Slip Vibrations Induced by Alternate Friction Models", Nonlinear Dynamics, Vol. 16, No. 1, pp. 41-51, 1998.

8. Olsen, J. E. and Irgens, F., "Aspects of Two Drum Winding", Proceedings of the Fourth International Conference on Web Handling, Oklahoma State University, Stillwater, Oklahoma, June 1-4, 1997.

9. Turner, R. N., "Empirical Analysis of Two Drum Winding", M.S. Thesis, Oklahoma State University, May 1997.

10. Reid, K. N., Tree, A., and Newton, J., "Seminar on The Analysis and Design of Web Transport Systems", Tab 1, Oklahoma State University, March 1996.

11. Dapcevic, D., Borthwick, K., and Fransen, P., "Structuring of Winder Drive Software: Review of Basic Building Blocks", IEEE Transactions on Industrial Applications, Vol. 35, No. 3, pp. 713-724, May/Jun. 1999.